Volume 38 | Number 5 | May 2014 | Pages 1811–2146

NJC

New Journal of Chemistry

www.rsc.org/njc

A journal for new directions in chemistry

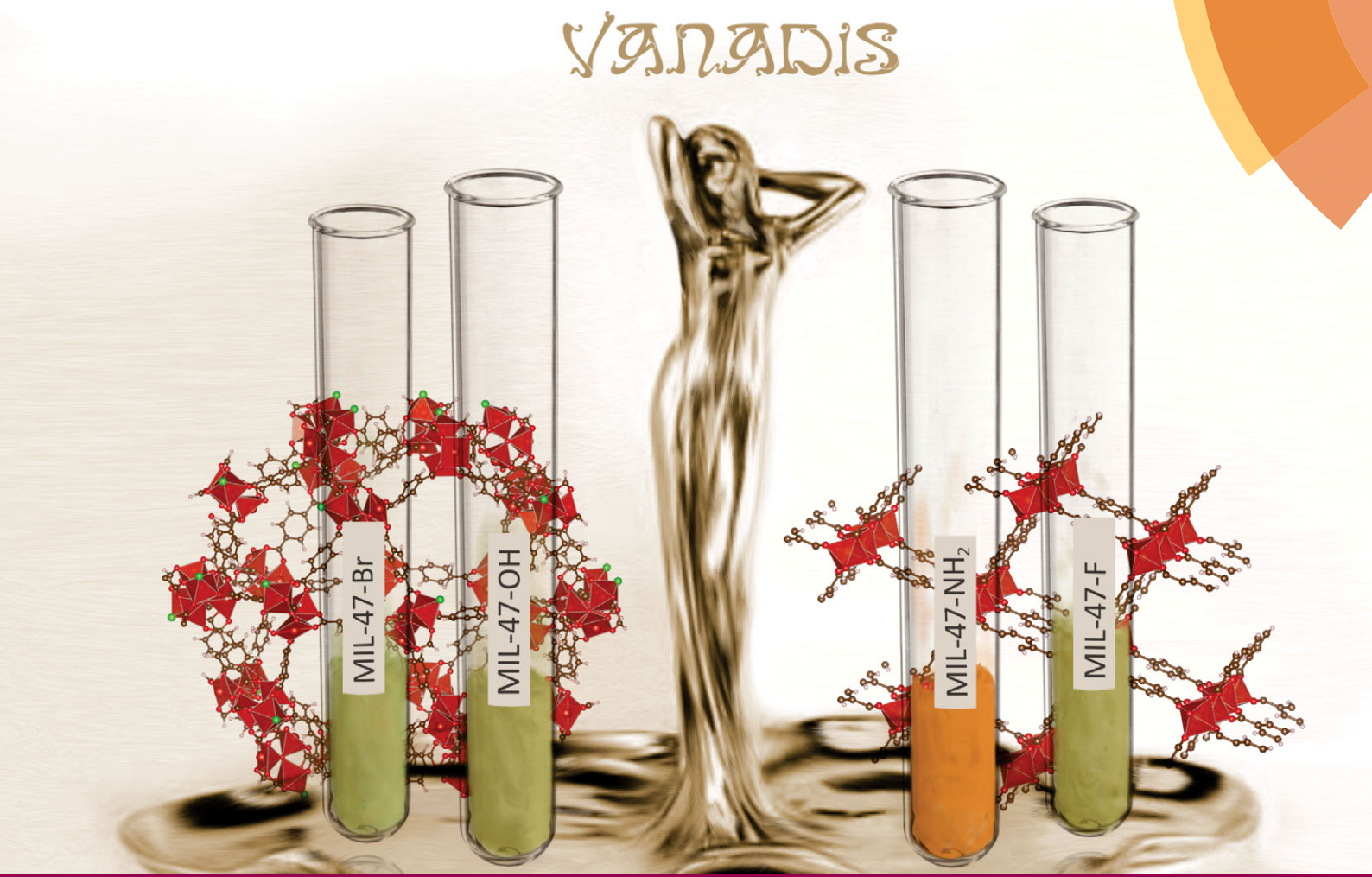

Themed issue: Advanced complex inorganic nanomaterials

ISSN 1144-0546

ROYAL SOCIETY OF CHEMISTRY

PERSPECTIVE

Pascal Van Der Voort *et al.*

Vanadium metal–organic frameworks: structures and applications

cnrs

NJC

PERSPECTIVE

View Article Online
View Journal | View Issue

Vanadium metal–organic frameworks: structures and applications

Cite this: *New J. Chem.*, 2014, **38**, 1853

Received (in Montpellier, France) 20th September 2013,
Accepted 1st November 2013

DOI: 10.1039/c3nj01130e

www.rsc.org/njc

Pascal Van Der Voort,*[a] Karen Leus,[a] Ying-Ya Liu,[a] Matthias Vandichel,[b] Veronique Van Speybroeck,[b] Michel Waroquier[b] and Shyam Biswas[a]

This perspective review paper describes the V-containing metal–organic frameworks that have been developed since the first systematic reports on MOFs almost 15 years ago. These hybrid crystalline materials, containing V(III) or V(IV) as metal nodes, show interesting behavior in oxidation catalysis and gas sorption. A significant amount of papers has appeared on the use of these structures in gas (hydrocarbon, CO_2) separation. Promising future research and development of V-MOFs is suggested.

Introduction

While MOFs based on divalent metals (Zn^{2+}, Cu^{2+}) have received much attention in the literature, fewer papers have appeared on trivalent or tetravalent metals in MOFs. And amongst these, the reported studies on vanadium MOFs are very rare. This is surprising, considering the wide range of clusters and complexes that can be formed with vanadium nodes.

[a] *Dept. of Inorganic and Physical Chemistry, Center for Ordered Materials, Organometallics and Catalysis, Ghent University, Krijgslaan 281 S3, 9000 Ghent, Belgium. E-mail: pascal.vandervoort@ugent.be*
[b] *Center for Molecular Modeling, Ghent University, Technologiepark 903, 9052 Zwijnaarde, Belgium. E-mail: veronique.vanspeybroeck@ugent.be*

In this review we describe all V-containing MOFs that have been reported to date, focusing on their structure, porosity and stability and discussing their applications in heterogeneous catalysis and sorption. Out of all the V-MOFs that have been fabricated, one variant – the so-called MIL-47 – receives most of the attention in the literature. A list of acronyms can be found at the end of this paper.

MIL-47 was the first porous vanadium based MOF reported in the literature.[1] This MOF is the most studied vanadium MOF because of its large specific surface area ($S_{Langmuir}$ = 1320 m^2 g^{-1}), high thermal stability (400 °C) in air and excellent catalytic activity in oxidation reactions. However, its stability in water is much lower than the isotopical Cr–MIL-53 or Al–MIL-53.[2]

Pascal Van Der Voort

Pascal Van Der Voort is a professor at Ghent University, Dept. of Inorganic and Physical Chemistry and had founded the research group COMOC in 2007 (www.we06.ugent.be/comoc). The core of this research group currently consists of 4 post-docs, 12 PhD students and 2 technicians. COMOC specializes in the synthesis of advanced and functional ordered porous materials (oxides, PMOs, MOFs, polymers) for various applications, emphasizing on adsorption and catalysis. Pascal Van Der Voort is the author of ~150 papers indexed in the Web of Science, a similar amount of conference proceedings and has authored several books.

Karen Leus

Karen Leus received her master's degree in Chemistry in 2007 at Ghent University and obtained her teaching degree in 2008 at Ghent University. In 2012 she completed her PhD in the research group COMOC under the supervision of Prof. Van Der Voort. During her PhD she worked on the synthesis and characterization of V-MOF materials for applications in adsorption and catalysis. In 2013 she gained a post-doctoral research grant from Ghent University for a research project on the synthesis of nanoparticles in MOFs for applications in catalysis.

Structure

The structures of only a few vanadium MOFs, namely MIL-47,[1,3] dimethyl-functionalized MIL-47 (also termed MOF-48),[4] MIL-59[5] and MIL-68,[6] were determined from single-crystal X-ray diffraction data.

Due to the difficulty in obtaining the single-crystals, the structures of the rest of the vanadium MOFs (see Table 1) were determined *ab initio* from their XRPD patterns collected using synchrotron or laboratory diffractometers. There are mainly two types of structural motifs (Fig. 1) found in vanadium MOFs: (i) chains of vanadium octahedra bridged by –OH groups and/or F atoms; and (ii) oxido-centered trimers of vanadium octahedra.

MOFs containing $\{V–O–V\}_\infty$ chains

The examples of MOFs that contain infinite chains of corner-linked $[V^{III}(OH)(R\text{-}(CO_2)_2)]$ octahedra in their as-synthesized forms include MIL-47,[1] COMOC-2,[9] COMOC-3,[10] MIL-60,[7] MIL-61,[7] MIL-68,[6] and MIL-71,[8] the representative structures are shown in Fig. 2. The octahedra are connected with each other by the polytopic carboxylate linkers to form three-dimensional frameworks having different types of topology. COMOC-2 bears the MIL-47 topology, whereas COMOC-3 has the MIL-69[13] topology. On the other hand, each of MIL-60, MIL-61, MIL-68 and MIL-71 possesses its own independent framework topology. The guest molecules, entrapped within the pores of the as-synthesized MOFs containing $\{V–O–V\}_\infty$ chains, are removed by thermal activation leading to the empty-pore forms. During thermal activation in air, the framework V^{3+} ions are oxidized to V^{4+} and the V^{III}–OH bonds are changed to a vanadyl (V^{IV}=O) group, but the topology of the frameworks remains unchanged. After calcination, permanent porosity has been achieved for MIL-47, COMOC-2, MIL-68 and MIL-71.

Ying-Ya Liu

Ying-Ya Liu received her PhD from Dalian Institute of Chemical Physics, Chinese Academy of Sciences, China in 2008. Since then, Dr Liu has been a post-doctoral researcher in Inorganic Chemistry II, Ulm University, under the supervision of Prof. Dirk Volkmer. From 2010, she worked as postdoc. at COMOC under the supervision of Prof. Pascal Van Der Voort. In October 2013, she joined the faculty at Dalian University of Technology (DUT), Dalian, China, where she is currently an associate professor in School of Chemical Engineering, DUT. Her current research interests are in the general area of metal–organic frameworks and their applications.

Matthias Vandichel

Matthias Vandichel, born in 1985, joined the Center for Molecular Modeling in 2007 for a master's thesis to unravel the generation of cyclic species during the initial stages of the methanol-to-olefins process. He obtained a degree in chemical engineering in 2008 and started his PhD research on nanoporous materials under the supervision of Prof. Waroquier and Prof. Van Speybroeck. In particular, he modeled reaction pathways of various catalytic systems and compared first-principles chemical kinetics with experimental data. He received his PhD in 2012 and continued his research activities related to the active site modulation of metal–organic frameworks.

Veronique Van Speybroeck

Veronique Van Speybroeck is full professor at the Ghent University within the faculty of engineering and architecture. She graduated as an engineer in physics and obtained her PhD in 2001. She is one of the founders of the Center for Molecular Modeling, which is currently composed of about 35 researchers. In this center, she is leading the computational molecular modeling division. Her research is focused on the kinetics of chemical reactions using molecular modeling techniques. In 2010, she received a European Research Council (ERC) starting grant on the topic "First principle chemical kinetics in nanoporous materials".

Shyam Biswas

Shyam Biswas completed his PhD in 2010 from University of Ulm under the supervision of Prof. Dirk Volkmer in the area of coordination compounds and coordination polymers based on 1,2,3-triazolate ligands. During 2010–2013, he has gained postdoctoral research experience with Prof. Norbert Stock and Prof. Pascal Van Der Voort at University of Kiel and University of Ghent, respectively, in the area of gas–vapor–liquid adsorption and catalytic applications of metal–organic frameworks. In 2013, he joined Indian Institute of Technology Guwahati as an assistant professor. His current research interests are the same as those of the postdoctoral time.

Table 1 Overview of the reported V-MOFs, acronyms for "Linkers" are described at the end of the paper

Entry	MOF	Building units	Space group	Crystal system	Porosity	Linker	Largest aperture	Ref.
1	MIL-47	$\{V–O–V\}_\infty$ chains	*Pnma*	Orthorhombic	Porous/non flexible	BDC	10.5 × 11 Å	1
2	MOF-48	$\{V–O–V\}_\infty$ chains	*Pnma*	Orthorhombic	Porous/non flexible	DMBDC	—	4
3	MIL-59	Oxido-centered vanadium trimers	*Pa*3	Cubic	Non porous	Isophthalic acid	—	5
4	MIL-68	$\{V–O–V\}_\infty$ chains	*Cmcm*	Orthorhombic	Porous/non flexible	BDC	—	6
5	MIL-60	$\{V–O–V\}_\infty$ chains	*P*1	Triclinic	Non porous	BTEC	—	7
6	MIL-61	$\{V–O–V\}_\infty$ chains	*Pnma*	Orthorhombic	Non porous	BTEC	—	7
7	MIL-71	$\{V–O–V\}_\infty$ chains	*Cmmm*	Orthorhombic	Porous/non flexible	BDC	—	8
9	COMOC-2	$\{V–O–V\}_\infty$ chains	*Imma*	Orthorhombic	Porous/flexible	BPDC	18.9 × 19.4 Å	9
10	COMOC-3	$\{V–O–V\}_\infty$ chains	*C*2/*c*	Monoclinic	Non porous	NDC	—	10
11	MIL-100	Oxido-centered vanadium trimers	$Fd\bar{3}m$	Cubic	Porous/non flexible	BTC	25 × 29 Å	11
12	MIL-101	Oxido-centered vanadium trimers	$Fd\bar{3}m$	Cubic	Porous/non flexible	BDC		12

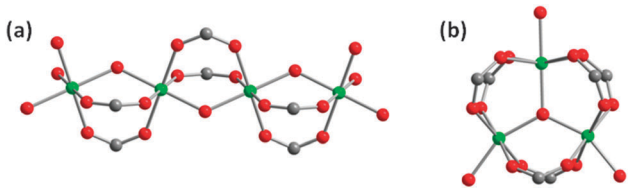

Fig. 1 Ball-and-stick representation of the two types of structural building units found in vanadium MOFs: (a) infinite trans chains of $[V^{III}(OH)_2O_4]$ octahedra and (b) oxo-centered trimers of vanadium octahedra. Color codes: V octahedra, green; C, grey; O, red.

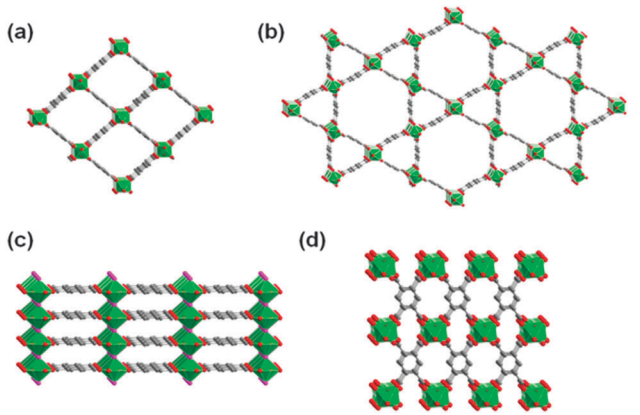

Fig. 2 Ball-and-stick representation of the 3D framework structures of (a) MIL-47, (b) MIL-68, (c) MIL-71 and (d) MIL-60. Color codes: V octahedra, green; C, grey; O, red. Crystal data taken from ref. 1–8.

However, COMOC-3, MIL-60 and MIL-61 possess narrow pore diameters and thus are non-porous towards nitrogen.

The 3D framework of MIL-47 (Fig. 2a)[1] contains 1D rhombic-shaped channels, each of which is delimited by four BDC linkers and four vanadium octahedra. Due to the absence of μ_2-OH groups, it exhibits a relatively rigid structure in its empty-pore form, as compared to M–MIL-53 (M^{III} = Al, Cr, Fe, Ga, Sc, In).[14] The pore dimensions of the as-synthesized and empty-pore forms of MIL-47 are 7.9 × 12.0 Å and 10.5 × 11.0 Å, respectively. A slight difference in the unit cell volumes (88 $Å^3$) between the as-synthesized and the empty-pore forms has been observed for MIL-47, indicating negligible flexibility as compared to M-MIL-53. COMOC-2 and COMOC-3 incorporate BPDC and NDC linkers, respectively. Thus, the dimensions of the rhombic-shaped channels of COMOC-2 (18.9 Å × 19.4 Å) are larger compared to MIL-47. However, COMOC-3 bears a flat 1D channel system with dimensions of only 2.7 × 19.4 Å. Thus, COMOC-3 displays a closed (non-porous) structure.

The framework structures of both MIL-60 and MIL-61 (Fig. 2d)[7] are constituted by the $\{V–O–V\}_\infty$ chains, which are cross-linked by the BTEC linkers forming channels or cages. In MIL-60, each BTEC linker is connected with four different octahedral chains through its four carboxylate groups. The connections between the linkers and the $\{V–O–V\}_\infty$ chains form intersecting channels. The channels along the *a*-axis show an almost square section with a free aperture of *ca.* 4 Å. However, the blockage of the pore aperture by the hydrogen atoms of the –OH groups renders the compounds non-porous. Compared to MIL-60, the BTEC linkers in MIL-61 have two non-coordinated carboxylate groups. MIL-61 shows a complex 3D structure having no accessible pore aperture for the entrance of nitrogen molecules. Thus, MIL-61 is also non-porous similar to MIL-60. In spite of having the same framework stoichiometry and bearing the identical octahedral $\{V–O–V\}_\infty$ chains, the framework topology of MIL-68 (Fig. 2b)[6] is completely different from MIL-47. The Schläffli symbol for the network of MIL-47 and MIL-68 is 4^4 and 6.3.6.3, respectively. The connectivity between the chains of octahedral $[V^{III}(OH)_2O_4]$ units and the BDC linkers in MIL-68 gives rise to a 3D Kagomé structure consisting of two types of 1D channels: small triangular channels built up of three chains and large hexagonal channels consisting of six chains. The trigonal and the hexagonal channels have free diameters of ~6 and ~16 Å, respectively.

Fluoride also acts as a bridging anion in MIL-71 (Fig. 2c),[8] in addition to the –OH groups bridging the vanadium octahedra as found in the above-described vanadium MOFs. The framework structure of MIL-71 is constructed from corner-linked $[V^{III}O_2(OH)_2F_2]$ octahedra and BDC linkers. The vanadium octahedra are bridged by –OH groups and F atoms along the *b* and *c* axis, respectively, to generate 2D layers of octahedra perpendicular to the *a* axis. The 2D inorganic layers are interconnected by the BDC linkers to form the 3D pillared-layered structure of MIL-71. The shortest distance between the phenyl rings is 3.8 Å, suggesting Π–Π interactions.

Structural flexibility of V-MOFs

The flexibility of some V-MOFs structures has been studied intensively. In 2011, Leclerc *et al.*[15] have developed an alternative

Table 2 Unit-cell dimensions and volumes of the flexible V-MOFs determined from X-ray powder diffraction

Compound		Space group	a (Å)	b (Å)	c (Å)	β (°)	V (Å^3)	P (MPa)	Comment	Ref.
MIL-47(V^{IV})	LP	Orthorhombic	16.059 (2)	13.963 (2)	6.815 (1)	—	1528.1 (3)	0.1	Cell contraction, 43%,	16
	NP	Monoclinic	21.117 (3)	6.710 (2)	6.717 (2)	114.41 (4)	866.6 (5)	340.1	induced by mechanical pressure	
MIL-47(V^{III})	LP	Orthorhombic	16.130 (1)	14.269 (1)	6.9087 (4)	90	1590.1 (2)	3.09	Cell contraction, 36%,	15
	NP	Monoclinic	19.858 (2)	7.6785 (8)	6.8404 (6)	104.40 (1)	1010.3 (2)	0.36	induced by CO_2 pressure at 303 K	
COMOC-2(V^{IV})	LP	Orthorhombic	6.651 (4)	27.94 (4)	10.735 (13)	97.06 (8)	1979.4 (47)	1.5	Cell contraction, 33%,	9
	NP	Monoclinic	6.776 (3)	23.087 (19)	18.897 (9)	90	2956.1 (32)	0.75	induced by CO_2 pressure at 233 K	

activation method to stabilize MIL-47 in the V^{III} oxidation state. They showed that, unlike MIL-47(V^{IV}), MIL-47(V^{III}) is a flexible structure with the μ_2-hydroxyl groups acting as preferential adsorption sites for H_2O or CO_2. Moreover, by controlling the oxidation, an intermediate porous solid with mixed oxidation states V^{III}/V^{IV} further proved that the presence of V^{IV} centers inhibits the flexibility to a large extent. In 2012, Yot *et al.* have demonstrated a large flexibility of the MIL-47(V^{IV}) upon mechanical pressure.[16] In 2013, the first vanadium MOF showing framework flexibility under mild conditions is COMOC-2(V^{IV}). In contrast to its rigid aluminum analogue denoted as DUT-5,[17] the isostructural COMOC-2(V^{IV}) undergoes structural transitions between LP and NP forms. The breathing behavior of COMOC-2(V^{IV}) is indicated by the presence of hysteresis loops in the adsorption–desorption isotherms of N_2 (−196 °C), CO_2 (−8 °C, high-pressure) and *n*-hexane (50 °C). Moreover, the *in situ* synchrotron XRPD patterns collected as a function of CO_2 pressure at −40 °C, clearly confirmed the reversible change in structure between the large pore and the narrow pore forms.[9]

A summary of the cell parameter and volumes of these flexible V-MOFs is shown in Table 2. These structures have shown remarkable structural flexibility, which can be introduced either by a certain CO_2 pressure at RT or 233 K under mild conditions, such as MIL-47(V^{III}) or COMOC-2(V^{IV}); or under high mechanical pressure (340 MPa), where MIL-47(V^{IV}) also shows flexibility. The cell contraction is in the range of 33–43%. Moreover, spectroscopic techniques have been applied to observe the structural flexibility. Within this field Leclerc *et al.* made a remarkable contribution. In their study the flexibility was observed by infrared spectroscopy and Raman spectroscopy.[15] For FT-IR, the shift of the band at 1016–1022 cm^{-1} (δ(C–H), ν_{18a} mode of the terephthalate species) was used to monitor the structural changes (Fig. 3A). The ν_{18a} band at 1016 cm^{-1} is characteristic of the NP form of MIL-47(V^{III}). When the structure changed to the LP form under vacuum, the ν_{18a} band shifts to 1022 cm^{-1}. For Raman spectroscopy, information on the flexibility of the V-MOF is obtained with the shift of the carboxylate bands (Fig. 3B). The symmetric ν_s(COO) band at 1440 cm^{-1} in the LP form shifts down to 1422 cm^{-1} in the NP form. Similar Raman shifts were also observed on COMOC-2, which are an indication of structural change.[9]

Many theoretical attempts have been made to rationalize the existence of structural transitions starting from microscopic grounds. They have not yet lead to a well determined rule of thumb whether a particular MOF is flexible or not. It is the result of a very complex interplay between different factors. An interesting and very promising model based on thermodynamic grounds has been established by some of the authors,[18] demonstrating that

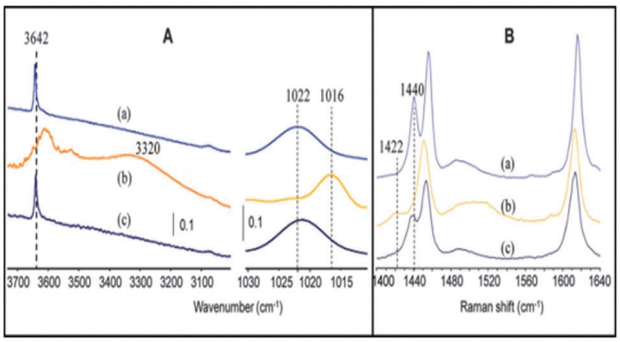

Fig. 3 Flexibility of MIL-47(V^{III}) upon hydration–dehydration evidenced by (A) FTIR (under vacuum) and (B) Raman (under gas flow): (a) after activation; (b) after exposure to water vapor; and (c) after dehydration at 453 K. Reproduced with permission from ref. 15. Copyright 2011 American Chemical Society.

a structural transition only occurs when the three contributions – host free energy, guest–guest and host–guest interactions – perfectly match some stringent constraints. The model has been successfully applied to Cr–MIL-53 but should be further validated for other porous MOFs. Theoretical efforts to rationalize breathing have also been made based on material properties. In this context, the work of Ortiz *et al.*[19] is of fundamental importance as it links quantum chemical results with mechanical properties of MOFs such as the elastic constants of the materials (Young's modulus, shear modulus, *etc.*), which can be extracted from the elasticity (or stiffness tensor). They are decisive in predicting the existence of structural transitions. It has been found that flexible MOFs are characterized by strong anisotropy of the Young's modulus.

MOFs containing oxido-centered vanadium trimers

Only three vanadium MOFs, namely MIL-59,[5] MIL-100[11] and MIL-101,[12] have been reported to date, which incorporate oxido-centered trimers of vanadium octahedra in their framework structures. The organic linkers in MIL-59, MIL-100 and MIL-101 are 1,3-benzenedicarboxylic acid (isophthalic acid), H_3BTC and H_2BDC, respectively. In MIL-59 (Fig. 4a),[5] water molecules act as the terminal ligands and the charge of the cationic cubic framework is balanced by the occluded chloride anions. Each trimer in MIL-59 is connected to six other similar trimers through six isophthalate anions. The resulting 3D framework of MIL-59 displays cuboidal cages delimited by eight trimeric building units with organic linkers on the walls.

The terminal ligands in MIL-100 are two water molecules and approximately one chloride anion per formula unit. On the

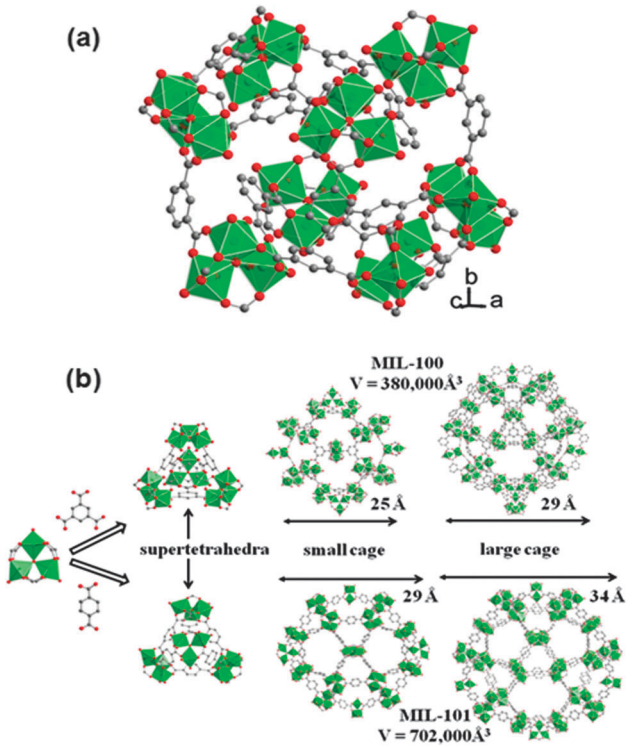

Fig. 4 (a) Ball-and-stick representation of a cuboidal cage of MIL-59 constructed from eight oxo-centered vanadium trimers. (b) The same representation showing the construction principles of the cage-like structures of MIL-100 and MIL-101. (left) A trimer of V octahedra and linkers (BTC for MIL-100 and BDC for MIL-101). (center) Hybrid supertetrahedra. (right) Smaller and larger cages of MIL-100 and MIL-101. Color codes: V octahedra, green; C, grey; O, red. Crystal data taken from ref. 5, 11 and 12.

other hand, MIL-101 possesses two DMF molecules and one chloride anion (per formula unit) as the terminal ligands. In both MIL-100 and MIL-101 (Fig. 4b),[11,12] the oxido-centered trimers are interconnected by the polytopic carboxylate linkers along the edges to form the so-called "supertetrahedra (ST)". In addition to the four vanadium trimers, the ST in MIL-100 and MIL-101 are built up of four and six organic linkers, respectively. The ST are further connected with each other in a three-dimensional fashion to yield the augmented zeolite Mobil Thirty-Nine (MTN) type of framework. Both of the networks of MIL-100 and MIL-101 contain two types of mesoporous cages (accessible cage diameters are 25 and 29 Å for MIL-100; 29 and 34 Å for MIL-101). The smaller and the larger cages contain 20 and 28 ST, respectively. The smaller cages consist of pentagonal windows and the larger cages include both pentagonal and hexagonal windows (free apertures of the pentagonal and the hexagonal windows are 4.8 and 8.6 Å for MIL-100; 12 and 16 Å for MIL-101).

Applications

Owing to their high specific surface area, pore volume and redox activity, vanadium MOFs have been extensively investigated in order to check their potential in adsorption–separation (gas, vapour and liquid) and heterogeneous catalysis.

Catalysis

Only a limited amount of catalytic studies on V-MOFs have been published so far. This is probably due to the rather small amount of reported V-MOFs which have a porous structure and a suitable oxidation state (V^{+IV} or V^{+V}). Moreover, the poor stability of these porous vanadium materials in aqueous or moist conditions does not encourage V-MOFs for broad use as catalysts. Almost all existing catalytic work on MIL-47 has been done by the experimental COMOC group and the CMM of the Ghent University. Their research was mainly focused on the liquid phase oxidation of cyclohexene with *tert*-butyl hydroperoxide (TBHP) as oxidant. The performance of the saturated vanadium MIL-47 was compared with that of the homogeneous but structurally resembling $VO(acac)_2$ catalyst.[20] Both catalysts showed an almost similar cyclohexene conversion and an analogous product distribution employing TBHP in water as oxidant (see Fig. 5a). When the catalytic performance of MIL-47 in the water based media is compared to the water-free media using TBHP in decane as the oxidant, the cyclohexene conversion is much lower in the water-free system as can be seen from Fig. 5b.[21] Nevertheless, a higher selectivity towards the cyclohexene oxide is observed (83%). Four consecutive runs were carried out to examine the regenerability of the catalyst using TBHP in decane as the oxidant. Although the TON and TOF dropped after the first run, they remain fairly constant in the additional runs. Furthermore, no leaching was observed during these extra runs and the crystalline structure was preserved.

The non-porous V-MOF, COMOC-3, was also examined for the liquid phase oxidation of cyclohexene employing TBHP in decane as oxidant. A similar cyclohexene conversion (38%) and selectivity towards the cyclohexene oxide (82%) was observed as for MIL-47 under the same reaction conditions. An extra V_4O_9 phase appeared after recalcination of COMOC-3 which could be attributed to the surface activation and bond breaking during the catalytic run combined with the oxidizing atmosphere of the calcination process.[10]

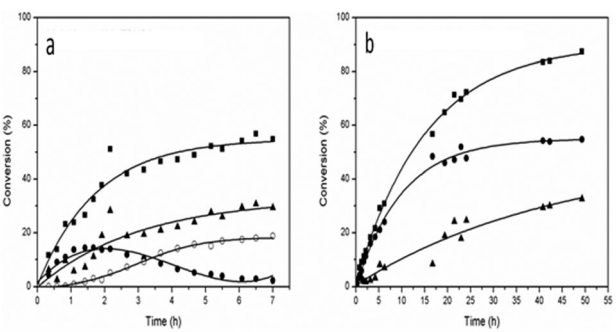

Fig. 5 Cyclohexene (**1**) conversion (■) and the yield of cyclohexene oxide (**2**) (●), *tert*-butyl-2-cyclohexenyl-1-peroxide (**4**) (▲) and cyclohexane-1,2-diol (**3**) (○) for MIL-47 in TBHP/water (left) with 0.42 mmol V-sites and in TBHP–decane (right) with 0.42 mmol V-sites. No cyclohexane-1,2-diol (○) is formed when TBHP–decane is used. The production of 2-cyclohexene-1-one is in all cases less than 5%, for the clarity of the figure this is not shown. Reproduced with permission from ref. 21. Copyright 2012 Elsevier.

A computational study was carried out to define the active catalytic sites and to propose a plausible reaction pathway for the epoxidation of cyclohexene, which was consistent with the observed findings. The experiments clearly revealed a similar cyclohexene conversion pattern for both the homogeneous $VO(acac)_2$–TBHP system and the porous MOF-type catalyst MIL-47, if the same amount of vanadium was used. As it involves the same metal and oxidant, the type of reaction paths in the heterogeneous catalytic process in MIL-47 should also be involved in the plethora of reactions taken place in a solution of vanadyl acetylacetonate ($VO(acac)_2$). The similar conversion curves, as observed experimentally, are the result of a compensation effect between the less accessibility of the V-sites in MIL-47 and the ligand effect (OAc ligand in the homogeneous catalytic process). The catalytic cycles occurring in the reaction mixture with the homogeneous catalyst $VO(acac)_2$ are very complex due to the presence of a large variety of complexes that can be formed, for example by ligand exchange reactions due to the presence of acetyl acetonate (acac), water, acetic acid, and the peroxide in the reagent mixture. A complete and thorough study on all possible pathways leading to the epoxidation of cyclohexene has been done by some of the authors.[22]

It has been shown that the concerted one-step Sharpless mechanism turns out to be the preferred reaction mechanism. Furthermore, the reagent mixture is composed of various inactive and active complexes. Inactive species are activated by the oxidant to form active complexes following the scheme displayed in Scheme 1. After epoxidation each active species transforms back into an inactive complex, which may be reactivated again. An additional element increasing the complexity of the whole process, is that the vanadium can reside in two oxidation states +IV and +V, and that radical decomposition reactions of active complexes can compete with the epoxidation reaction, at any moment switching from the V^{+IV} platform to the V^{+V} platform of active and inactive species, and *vice versa*. The interconversion of vanadium +V into +IV species is described as an equilibrium reaction on the Gibbs free energy surface and the reaction free energy is strongly competitive with the epoxidation free energy barrier, but varies a lot with the choice of the ligand.

The reaction mechanism in MIL-47 shows large similarities, but the selection of relevant pathways is much more limited.[22] First, free coordination positions should be created by ligand removal, sometimes accompanied by breaking the oxygen bond between the neighboring vanadium centers from the O–V–O axis. Active coordination sites are thus located at the edges or within the material. Then the reaction cycle starts with an activation step in which the TBHP coordinates to the V-center to form an alkylperoxo species **7** from which the two most probable reaction routes start as can be seen from Scheme 2. The first pathway is a direct pathway that leads to the formation of the cyclohexene oxide **2** and consequently bringing the catalyst to a less active complex **8**. Besides this direct epoxidation pathway a radical mechanism is plausible in which the V center is oxidized from V^{+IV} to V^{+V} by a homolytic cleavage of the peroxy linkage which can be further activated with TBHP. The activated complexes **10** and **12** can again epoxidize cyclohexene (**10** → **11** and **12** → **11**). Based on thermodynamical and kinetic grounds these pathways, which proceed through a vanadium in oxidation state +V, become the rate determining step in the epoxidation, yielding a free energy barrier of about 90 kJ mol^{-1} at T = 323 K. This agrees quite well with the experimental value of 80 kJ mol^{-1} measured in the epoxidation

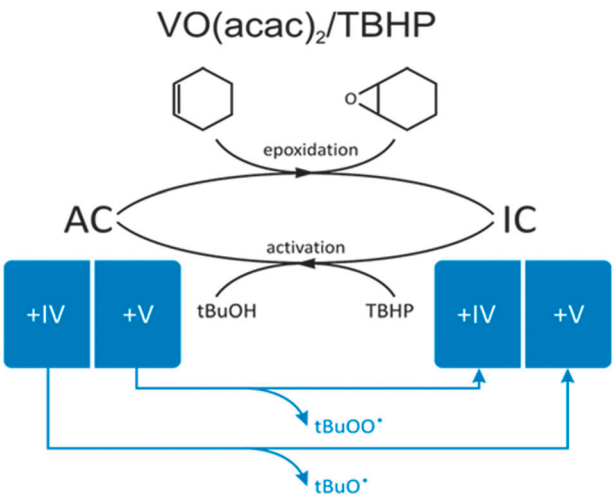

Scheme 1 Overview of the reaction scheme taking place in the cyclohexene epoxidation at the homogeneous $VO(acac)_2$ catalyst with TBHP as oxidant. The catalytic cycle consists of a consecutive transformation of active to inactive complexes and *vice versa*, constantly switching from oxidation state of the vanadium. Reproduced with permission from ref. 22. Copyright 2012 Elsevier.

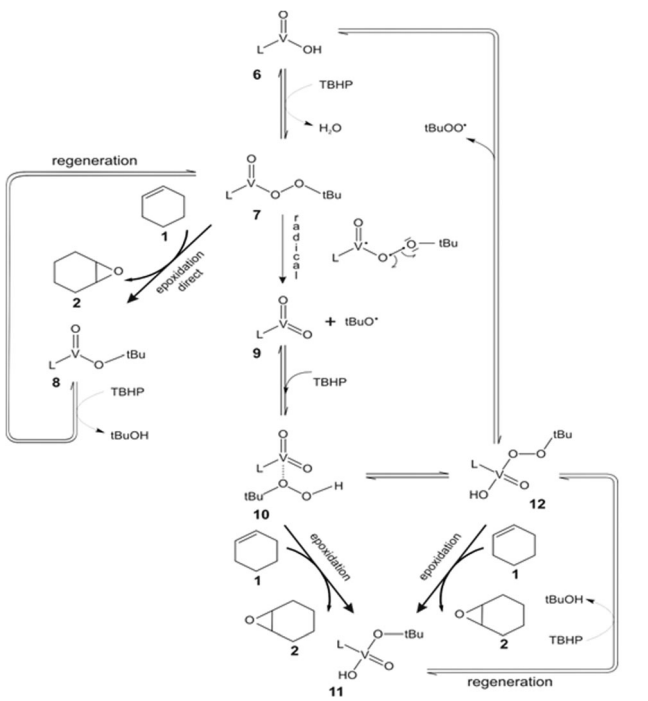

Scheme 2 Two competitive cyclohexene epoxidation pathways for MIL-47 (direct and radical) (V^{+IV} in cycle **7** → **8**; V^{+V} in cycle **10** → **11** and **12** → **11**). Reproduced with permission from ref. 21. Copyright 2012 Elsevier.

of cyclohexene with $VO(acac)_2$. In conclusion, the cyclohexene conversion in MIL-47 is of the same order as that observed using a homogeneous $VO(acac)_2$ catalyst.

In a recent study, the MIL-47–NH_2 was post-modified with a Ti-complex, $TiO(acac)_2$.[23] Molecular oxygen was used as the oxidant in combination with cyclohexanecarboxaldehyde as the co-oxidant. A faster and higher conversion is observed for the bimetallic MOF, in comparison to the unmodified MIL-47–NH_2. Both materials showed only 2 products: cyclohexene oxide and cyclohexene-1-one, which were produced in almost equal amounts.

Yaghi *et al.* evaluated MIL-47 and MOF-48 as a catalyst in the conversion of methane to acetic acid. In the absence of CO, the major product is acetic acid (the yield is 70% and 48% for respectively MIL-47 and MOF-48).[4] The authors attribute the higher yield of MIL-47 to the more open pores in comparison to MOF-48. The latter showed a higher selectivity towards methyl trifluoroacetate due to the more hydrophobic pores. By carrying out the reaction in the presence of CO, the amount of oxidant $K_2S_2O_8$ could be reduced while the amount of acetic acid and selectivity could be significantly enhanced.

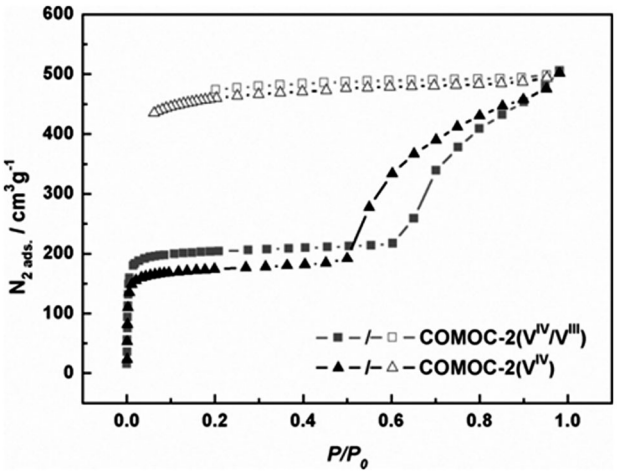

Fig. 6 N_2 adsorption (solid symbols) and desorption (open symbols) isotherms of COMOC-2(V^{IV}) (black) and COMOC-2(V^{IV}/V^{III}) (gray) at 77 K. Reproduced with permission from ref. 9. Copyright 2013 American Chemical Society.

Adsorption and/or separation of N_2, CO_2, CH_4

Nitrogen. The N_2 adsorption in most of the vanadium MOFs at −196 °C followed reversible type-I isotherms, which is characteristic of microporous solids. In contrast, small sub-steps below p/p_0 = 0.2 were observed in the N_2 adsorption isotherms of MIL-100, MIL-101 and MIL-101–NH_2.[11,12] The occurrence of these sub-steps in the type-I adsorption isotherms were attributed to the presence of mesoporous cages in their structures. Distinct hysteresis loops were observed in our recently reported COMOC-2(V^{IV}) and COMOC-2(V^{IV}/V^{III}) solids, which have been attributed to the structural transition of these MOFs upon adsorption of N_2 at −196 °C.[9] As shown in Fig. 6, though both COMOC-2(V^{IV}) and COMOC-2(V^{IV}/V^{III}) exhibited two-step N_2 adsorption isotherms, the first plateau was maintained up to p/p_0 values of 0.5 and 0.6, respectively. Thus, the presence of V^{III} atoms in COMOC-2(V^{IV}/V^{III}) compared to pure COMOC-2(V^{IV}) increased the difficulty in triggering the flexibility of the framework. The necessity of a higher N_2 pressure for COMOC-2(V^{III}/V^{IV}) to open up the pores has been attributed to the remaining internal stabilization effects (*e.g.*, H-bonding).

CO_2. High CO_2 adsorption capacities were achieved for a variety of vanadium MOFs. The specific BET surface area, CO_2 and CH_4 uptake values of the representative vanadium MOFs are summarized in Table 3. The highest specific BET surface area (2320 $m^2\ g^{-1}$) and thus the largest CO_2 uptake capacity (14.2 mmol g^{-1}) were obtained for V–MIL-100.[11] This CO_2 uptake capacity is in agreement with those of the isostructural MIL-100(Al, Cr, Fe) solids with similar BET surface areas.

The vanadium analogues of MIL-101 and MIL-101–NH_2 show significantly lower CO_2 uptake values compared to their chromium and aluminium analogues.[12] This difference was ascribed to the difficulty of removing the occluded solvent molecules from the pores of the vanadium MOFs due to their lower thermal stability, which results in a considerable decrease in the accessible surface areas. MIL-47 showed considerable CO_2 uptake capacity (11.5 mmol g^{-1}), which is

Table 3 BET surface area, CO_2 and CH_4 uptake values for representative vanadium MOFs as well as their aluminium and chromium analogues

MOF	S_{BET}[a] ($m^2\ g^{-1}$)	CO_2 uptake (mmol g^{-1})	CH_4 uptake (mmol g^{-1})	Uptake pressure (bar)	Uptake temp. (°C)	Ref.
MIL-47	930	11.5	5.6	CO_2:20.0/CH_4:25.0	CO_2:31/CH_4:30	24, 30
Al–MIL-53	1140	10.2	5.8	25.0	CO_2:31/CH_4:30	29, 31
Cr–MIL-53	—[b]	10.0	5.8	25.0	CO_2:31/CH_4:30	24
MIL-47–F	852	6.8	—	25.0	30	28
MIL-47–NH_2	535	6.1	2.8	25.0	30	27
MIL-47–OCH_3	637	8.3	—	21.5	30	29
COMOC-2	—[c]	4.4	1.6	25.0	30	9
V–MIL-100	2320	14.2	5.3	25.0	30	11
Fe–MIL-100	~2000	12.5	4.4	25.0	30	11
Cr–MIL-100	~2000	15.2	5.3	25.0	30	11
V–MIL-101	2118	9.0	—	24.5	27	12
Cr–MIL-101	4100	26	8.0	25.0	30	26
V–MIL-101–NH_2	1623	4.3	—	22.8	27	12
Al–MIL-101–NH_2	2100	14	5.0	CO_2:30.0/CH_4:25.0	25	31

[a] The specific BET surface areas have been calculated from the N_2 adsorption isotherms. [b] The Langmuir surface area of Cr–MIL-53 is 1500 $m^2\ g^{-1}$. [c] The N_2 uptake capacity of COMOC-2 at p/p_0 = 0.98 is 510 $cm^3\ g^{-1}$.

comparable to its structurally related MIL-53(Al, Cr) materials having comparable specific surface areas.[24] The adsorption of CO_2 in these materials has also been extensively examined in a DFT study by Ramsahye *et al.*[25] The principal goal of that paper was to better understand the mechanism of the CO_2 adsorption and to explore the possible adsorption sites. Geometry optimization of the framework loaded with 1 and 2 CO_2 molecules per unit cell has been performed using periodic calculations. The authors employ PW91 GCA as density functional but don't include dispersion effects. MIL-47 is isostructural to MIL-53lp but does not exhibit any structural transition upon CO_2 adsorption. The absence of a μ_2-OH in MIL-47 lies on the basis of fundamental differences in the nature of the CO_2 interaction with the framework. It means that in MIL-47 no preferential sites are found for CO_2 adsorption (Fig. 7).

Recently, Llewellyn and coworkers emphasized the importance of MIL-47 compared to other MOFs for CO_2 adsorption and CO_2–CH_4 separation.[26] Amongst the studied MOF-materials, MIL-47 was found to have the highest working capacity between 1 and 6 bar at 303 K. With operando infrared experiments, they could characterize the strength of the microscopic interactions in play and found an adsorption enthalpy of around -27.6 kJ mol^{-1}, which is similar to the values obtained *via* microcalorimetry (-20 to -25 kJ mol^{-1}).[26] This relatively weak enthalpy of adsorption suggests that no specific adsorption sites are present in the MIL-47 sample for the CO_2 quadrupole to interact with. They also observed that for a binary mixture of CO_2 and CH_4 the presence of methane does not impact the microscopic mechanism for CO_2. By using functionalized linkers, the working capacity might increase further.

The fluoro- and amino-functionalized MIL-47 exhibited high CO_2 uptake values, which are lower compared to the un-functionalized material.[27,28] Noticeable CO_2 adsorption capacities of 8.3 mmol g^{-1} have been obtained for the methoxy-modified MIL-47 solid.[29]

The high pressure CO_2 adsorption–desorption isotherms of un-functionalized MIL-47 and functionalized MIL-47–X (X = –F, –NH_2, –OCH_3) solids at ambient temperature displayed type-I adsorption behavior without the occurrence of any hysteresis loop, which was observed for its isostructural MIL-53(Al, Cr) solids.[29] The difference in shapes of adsorption isotherms was ascribed to the structural flexibility of MIL-53(Al, Cr) solids having μ_2-OH groups acting as preferential adsorption sites for CO_2, which are replaced by μ_2-O groups in rigid MIL-47(V^{IV}). Recently, the empty-pore MIL-47(V^{III}) material was obtained by thermal activation under vacuum, which showed two-step CO_2 adsorption isotherms at 30 °C. MIL-47(V^{III}) contains μ_2-OH groups in its framework and thus shows structural flexibility upon adsorption of CO_2, which has been verified *in situ* by coupled synchrotron XRPD–Raman techniques. In spite of lacking μ_2-OH groups, the recently reported COMOC-2(V^{IV}) solid also exhibited a hysteresis loop in the CO_2 adsorption–desorption isotherms (Fig. 8) at -8 °C due to structural transformation between large and narrow pore forms.[9] This structural transition was characterized by *in situ* synchrotron XRPD measurements upon dosing of CO_2 and by molecular simulations. At 30 °C, no hysteresis loop was observed in the CO_2 sorption isotherms of this material. However, the occurrence of hysteresis loops in the CO_2 sorption isotherms was not reported for DUT-5(Al^{III}), which is isostructural to COMOC-2(V^{IV}). Theoretically, a free energy profile for the empty host framework has been calculated for different temperatures using the periodic code VASP. Apart from a regular large pore and narrow pore, an additional overstretched narrow pore form has also been found. However this structure can never be reached with the presence of guest molecules and hence cannot be observed experimentally.

Methane. The CH_4 adsorption in all vanadium MOFs followed type-I isotherms. No hysteresis loop was noticed in the flexible vanadium MOFs MIL-47(V^{III})[15] and COMOC-2(V^{IV})[9] (Fig. 8), even when the temperature was significantly lowered. Similar CH_4 sorption behavior was also reported for MIL-53(Al, Cr).[30] The CH_4 adsorption capacities (Table 3) of MIL-47 and MIL-100 at 25 bar and 30 °C are 5.3 and 5.6 mmol g^{-1}, respectively.[30] These uptake

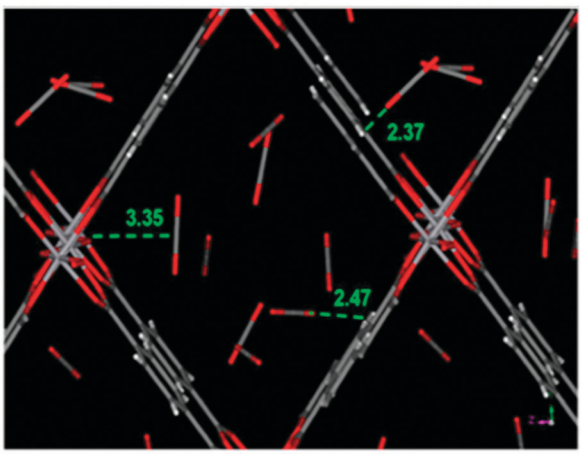

Fig. 7 A typical illustration of the CO_2 arrangement in the MIL-47 structure at high loading corresponding to 8 molecules per unit cell. The reported distances are in Å. Although some molecules interact with the framework, there are no preferential adsorption sites. Reproduced with permission from ref. 25*a*. Copyright 2007 Springer.

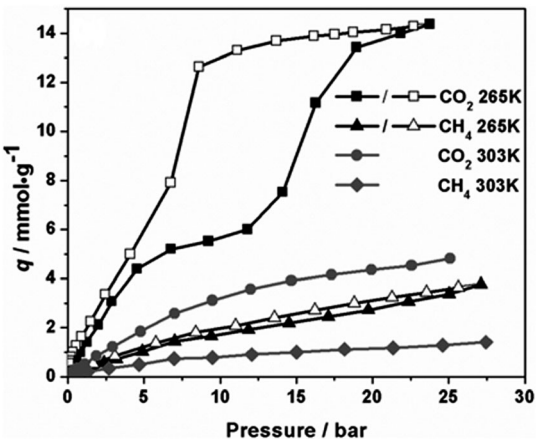

Fig. 8 Adsorption (solid symbol) isotherms of COMOC-2(V^{IV}) for CO_2 and CH_4 at 303 and 265 K. Desorption isotherms (open symbol) of CO_2 and CH_4 at 265 K are also included. Reproduced with permission from ref. 9. Copyright 2013 American Chemical Society.

values are also comparable with those of MIL-53(Al, Cr) solids (5.8 mmol g^{-1}). Much lower CH_4 uptake values of 1.6 and 2.8 mmol g^{-1} have been found for COMOC-2 and MIL-47–NH_2,[27] respectively.

CO_2–CH_4 separation. The adsorption and separation of CO_2 and CH_4 in MIL-47–NH_2 was investigated in a combined experimental and theoretical approach.[27] In the low pressure region, the CO_2 or CH_4 adsorption isotherms of MIL-47 and MIL-47–NH_2 coincided, indicating similar affinities of both materials towards CO_2 or CH_4. The adsorption enthalpies, Henry adsorption constants and separation factors of CO_2 and CH_4, calculated from low coverage pulse chromatographic experiments, were also similar for both materials. In contrast, the adsorption enthalpies of Al–MIL-53 and Al–MIL-53–NH_2 differed significantly and the separation factors were enhanced in orders of magnitude due to amination of Al–MIL-53.[32] The narrower pore size was attributed to the higher adsorption enthalpy of Al–MIL-53–NH_2 as compared to parent Al–MIL-53, which exhibited large pore form under the same experimental conditions. Due to their rigid structures, the adsorption properties of both MIL-47 and MIL-47–NH_2 are similar to MIL-53 in the low coverage region. The slight increase in adsorption enthalpy for MIL-47–NH_2 fails to compensate for the loss in pore volume compared to pristine MIL-47. This results in comparable CO_2–CH_4 separation factors for MIL-47 and MIL-47–NH_2. The CO_2–CH_4 adsorption selectivities, calculated from the breakthrough experiments, were also comparable for both materials and they were in agreement with the Henry selectivities. Moreover, the theoretical adsorption enthalpies followed the same trend as the experimental ones.

In a comprehensive study, the adsorptive performance of MIL-47 for CO_2 related applications was compared with other well-known MOFs (DUT-9, MOF-177, Cr–MIL-101, Al–MIL-53, $Cu_3(BTC)_2$), the activated carbon F400, and the zeolite NaY in both amount and volume adsorbed scales.[26] In terms of amount adsorbed in mmol g^{-1}, the CO_2 uptake value of MIL-47 was slightly higher compared to NaY. The CO_2 adsorption capacity of MIL-47 was found to be similar to Al–MIL-53 and F400. However, MIL-47 adsorbed a less amount of CO_2 than any other reference MOF material and almost 4 times less than the best MOF material Cr–MIL-101 at 50 bar. In order to evaluate MOFs with respect to processes such as PSA, it is relevant to compare the materials in terms of volume adsorbed per volume of materials. This is owing to the fact that the MOF will presumably be packed in a given bed volume. On the volume per volume basis, MIL-47 and Cr–MIL-101 showed almost similar CO_2 uptake capacities at 50 bar. Interestingly, the CO_2 uptake of Al–MIL-53 in terms of volume per volume was 30% lower than that of MIL-47 owing to the breathing effect. Even on this scale, the selected MOF materials displayed higher total CO_2 uptakes than NaY. Because of the lack of any specific adsorption site, MIL-47 showed moderate CO_2–CH_4 selectivity values, similar to many activated carbon materials, and not as good as MOFs with open metal sites such as MIL-100[33] or most zeolites. Nevertheless, the high volumetric working capacity of MIL-47, which is comparable with that of $Cu_3(BTC)_2$, might make it a potential material in some CO_2 separation processes.

In another rigorous study, the potential of several MOFs (MIL-47, Cr–MIL-100, MIL-140A, $Cu_3(BTC)_2$ and Cr–MIL-53) as CO_2 adsorbents in PSA processes were compared with reference adsorbents such as zeolite NaX and activated carbon AC35.[34] For the same reason, MIL-47 and MIL-140A showed lower affinity towards CO_2 compared to the other MOFs. The CO_2–CH_4 breakthrough experiments showed that the separation decreases in the order: NaX > $Cu_3(BTC)_2$ > Cr–MIL-100 > MIL-47 ≈ AC35 ≫ MIL-140A.

On the other hand, the breakthrough curves for the ternary CO_2–CH_4–CO mixtures revealed the following descending order of separation: NaX > $Cu_3(BTC)_2$ > MIL-47 ≈ AC35 > Cr–MIL-100 ≫ MIL-140A. The simulated plot of separation factor *vs.* working capacity for biogas separation (50 : 50 mixture CO_2–CH_4; feed at 10 bar, desorption at 1 bar) revealed that the best separation can be achieved by NaX. Cr–MIL-100 and MIL-47 showed similar separation factors to $Cu_3(BTC)_2$, but lower working capacities. The lower working capacity of Cr–MIL-100 was attributed to the huge pore volume, which is not efficiently filled at 5 bar. Moreover, the open metal sites in Cr–MIL-100 are difficult to regenerate at 1 bar. From the simulated plot of separation factor *vs.* working capacity for CO_2 capture in H_2 purification and in IGCC systems (Fig. 9), the best CO_2–CH_4–CO separation factors (feed at 28 bar, desorption at 1 bar) were observed for MIL-47 and NaX. Both Cr–MIL-100 and $Cu_3(BTC)_2$ showed lower CO_2–CO separation factors, which was ascribed to the favorable interaction of the open metal sites with CO. These simulated separation factors were in agreement with the experimental breakthrough curves. The estimated adiabatic working capacity of MIL-47 and Cr–MIL-100 were higher compared to the other MOFs, which was assigned to the lower adsorption enthalpy of the former and high heat capacity of the latter. Nevertheless, if long term stability is considered, the applications of the otherwise potential MIL-47 and $Cu_3(BTC)_2$ in PSA applications might be hampered.

Diffusion of methane gas (CH_4) through the pores of Cr–MIL-53 and MIL-47 has also been investigated by the experimental–theoretical group of Ferey and Maurin.[35] Molecular

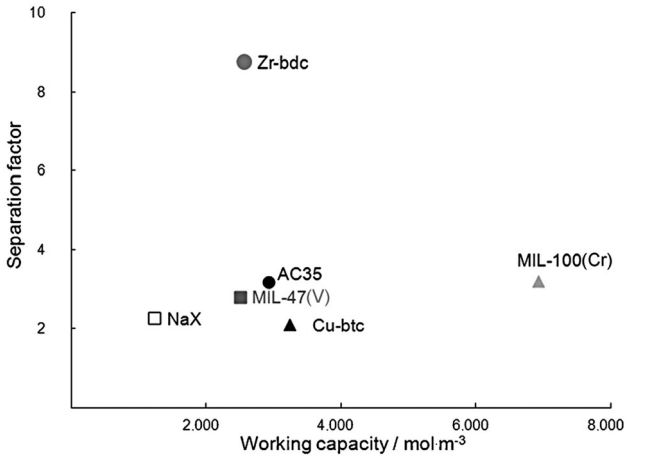

Fig. 9 Separation factor *vs.* working capacity of various MOFs, activated carbon AC35 and zeolite NaX for CO_2 capture in IGCC systems. Adsorption pressure: 57 bar, desorption pressure: 5 bar. Reproduced with permission from ref. 34. Copyright 2012 Wiley-VCH Verlag GmbH & Co. KGaA.

dynamics simulations are also able to extract self-diffusion coefficients in MOFs. It has been found that the CH_4 mobility in the two MILs has never been observed that high in other MOFs and zeolites with large pores such as NaY. About the adsorption sites of CH_4 in the two MILs, the same conclusions can be drawn as for CO_2.

Adsorption of alkanes and alkenes

The adsorption of short and long-chain linear/branched alkanes in MIL-47 has been extensively investigated. In a comparative study, the adsorption properties of *n*-hexane and *n*-nonane in MIL-47 was compared with those in Cr–MIL-53.[36] Large uptakes were achieved at low relative pressures for both compounds, which indicated strong adsorbate–adsorbent interactions due to confinement effects inside the micropores. At 40 °C, MIL-47 showed type-I adsorption isotherms having high uptake values of 3.7 and 2.0 mmol g^{-1} for *n*-hexane and *n*-nonane, respectively. The *n*-hexane and *n*-nonane adsorption capacity of Cr–MIL-53 at 40 °C reached 2.0 and 1.6 mmol g^{-1}, respectively.

Computational methods can play a useful role to deepen our understanding of the whole adsorption mechanism at the atomic level. Most of the molecular simulation studies are based on Monte-Carlo calculations, and more particularly Grand Canonical Monte Carlo (GCMC) simulations using force fields. This methodology has been applied by the group of G. Maurin to a broad selection of adsorbates. They systematically combine molecular simulations with microcalorimetry–gravimetry experiments. For short-chain linear alkanes (methane to *n*-butane) adsorbates, no significant structural modification of the MIL-47 framework has been noticed, highlighting its rigid character.[30] The calculations also reveal that MIL-47 does not exhibit any preferential adsorption sites. For linear long-chain alkanes (*n*-pentane to *n*-nonane)[37] the experimental adsorption isotherms (Fig. 10) of the C_5 to C_9 alkanes are of type-I, consistent with the rigid nature of microporous MIL-47 solid. The saturation capacities reached 4.2, 3.8, 3.2, 2.7 and 2.1 mmol g^{-1} for *n*-pentane, *n*-hexane, *n*-heptane, *n*-octane and *n*-nonane, respectively. A fair agreement of the experimental absolute adsorption isotherms and enthalpies of adsorption with those of the simulated ones was achieved. Both experimental and simulated adsorption enthalpies evolved linearly with an increase in the carbon number of the alkyl chain, as observed formerly for short-chain linear alkanes.[30] The MD simulations revealed that the *n*-alkane molecules followed a pathway along the channel, resulting in a 1D-type diffusion mechanism. At low loading, the motions of the molecules were centered around the middle of the pores, whereas they were increasingly shifted towards the pore wall at higher loadings.

Recently, we have investigated the *n*-hexane adsorption properties of the isostructural, mono-fluorinated MIL-47 and Al–MIL-53 solids.[28] The *n*-hexane adsorption isotherms of both materials exhibited type-I isotherms. In contrast to parent Al–MIL-53, no sub-step was observed in the *n*-hexane adsorption isotherms of Al–MIL-53–F. It was concluded that the fluorination suppressed the structural transformation of Al–MIL-53–F upon the adsorption of *n*-hexane. The *n*-hexane uptake values of MIL-47–F and Al–MIL-53–F at 50 °C and p/p_0 = 0.5 reached

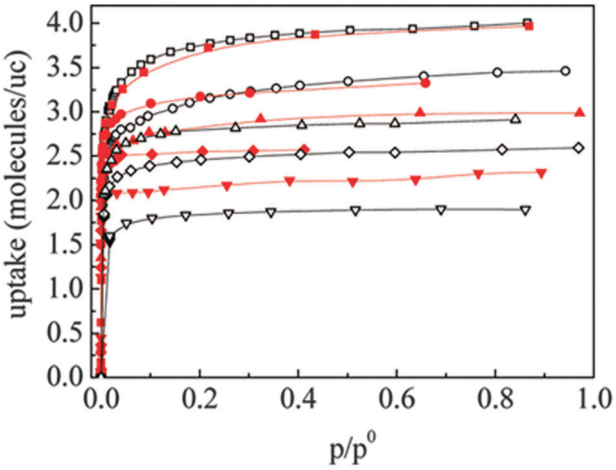

Fig. 10 Comparison between the experimental (empty symbols) and simulated (filled symbols) adsorption isotherms for *n*-pentane (squares), *n*-hexane (circles), *n*-heptane (triangles), *n*-octane (diamonds), and *n*-nonane (upside down triangles). The simulated data were obtained using model 2. Reproduced with permission from ref. 37. Copyright 2011 American Chemical Society.

2.3 mmol g^{-1} for each solid, which is lower compared to that of pristine MIL-47 (3.6 mmol g^{-1})[36] and Al–MIL-53 (2.9 mmol g^{-1})[38] at 40 °C and p/p_0 = 0.5. More recently, we also prepared and tested the difluorinated variants of MIL-47(V) and MIL-53(Al).[39] The fluorination induces noticeable hydrophobicity in both of the difluorinated compounds, as demonstrated by the H_2O sorption experiments. The *n*-hexane adsorption capacity of difluorinated MIL-47 at 50 °C and p/p_0 = 0.5 exceeds that of parent MIL-47 owing to the enhanced hydrophobicity achieved through fluorination of the framework. We have also explored the *n*-hexane adsorption behavior of the structurally flexible COMOC-2 material.[9] At 50 °C, this solid exhibited a two-step adsorption isotherm, which was explained by the structural transition. The *n*-hexane adsorption capacity of COMOC-2 at saturation pressure reached as high as 4.7 mmol g^{-1}.

Low-coverage adsorption properties of linear and branched alkanes were also determined in a combined experimental and GCMC study.[40] For each additional $-CH_2$ group, the experimental Henry adsorption constants increased linearly with a factor of 2.8 for the linear alkanes and a factor of 2.7 for the branched alkanes. The branched alkanes displayed slightly lower Henry adsorption constants compared to the linear alkanes. Moreover, the experimental and simulated adsorption enthalpies of the branched alkanes were slightly lower than those of the linear alkanes. Thus, the linear alkanes were preferentially adsorbed over the branched alkanes. Generally, the branched alkanes show less close contact of all H atoms with the framework due to the presence of side methyl groups. However, it was emphasized that the branched alkanes were not influenced by steric constrains from the MIL-47 framework. The simulations showed that both linear and branched alkanes adsorb in the center of the pores and not near the metal centers or the pore walls. Like any other microporous material, the experimental and simulated adsorption enthalpies for MIL-47

increased linearly with carbon number of the alkyl chain due to the additional dispersive interactions induced by every additional $-CH_2$ group. An increase of 7.6 kJ mol^{-1} was observed experimentally for each additional $-CH_2$ group, which compared well with an increase of 7.8 kJ mol^{-1} in the simulations. The experimental and simulated separation factors for a mixture of linear and branched alkanes were low, indicating the absence of shape selectivity in MIL-47.

The selective adsorption of alkenes was investigated in MIL-47, Al–MIL-53 and $Cu_3(BTC)_2$.[41] Only $Cu_3(BTC)_2$ was able to adsorb significant amounts of alkenes, whereas MIL-47 and Al–MIL-53 showed negligible uptakes from hexane. Since no steric hindrance is expected from the later two solids, the presence of open metal sites in $Cu_3(BTC)_2$ appears to be beneficial for the adsorption of alkenes.

Adsorption, diffusion and separation of aromatic and heterocyclic compounds

We will first discuss the diffusion of benzene through the pores of MIL-47, which shows some spectacular features: the benzene molecule moves in a corkscrew fashion and rotates about its C_2 axis parallel to the channel axis (see Fig. 11). This has been established by combining experimental (quasielastic neutron scattering and ^2H NMR) and theoretical tools.[42] This picture learns that the aromatic diffuses along the 1D channels, while randomly rotating by 90° jumps, thus performing a corkscrew motion.

In a later stage, the same group (Maurin–Ferey) applied the same techniques to study the dynamics of xylene isomers in MIL-47.[43] They found a similar 1D diffusion mechanism as observed for benzene in the low temperature range, while at higher temperature the confined species is subjected to a jump-diffusion motion along the channel center crossing barriers which are low in energy.

Separation of *para*-xylene from the other *o*- and *m*-isomers is one of the challenging issues in the chemical industry. MIL-47 has demonstrated its ability in selectively adsorbing xylene isomers, and most of the experimental work on these issues has been done by the COK-Leuven group. In the following, a short overview will be given.

First, the *liquid-phase* adsorption and separation of xylene isomers and ethylbenzene (EB) in MIL-47, Al–MIL-53 and $Cu_3(BTC)_2$ were explored.[44] $Cu_3(BTC)_2$ showed poor selectivities, except for *m*-xylene *versus* *o*-xylene. In contrast, both MIL-47 and Al–MIL-53 showed remarkable preference for *p*-xylene over EB. The selectivity of MIL-47 for *p*-xylene over EB reached 9.7 : 1. In addition, MIL-47 also preferred *p*-xylene over *m*-xylene with a selectivity of 2.9 : 1, whereas Al–MIL-53 did not exhibit any preference for these two isomers. The *para*-selectivity of MIL-47 was also confirmed by pulse chromatographic and breakthrough experiments. The zero coverage adsorption enthalpies of all the C_8 aromatic compounds were almost identical, which indicated that molecular packing rather than adsorbate–framework interactions determined the observed selectivities in the sterically confining channels of MIL-47. This was also the conclusion of a GCMC calculation using standard force fields by Castillo *et al.*[45] The Rietveld analyses (Fig. 12) of the XRPD patterns of MIL-47 saturated with the C_8 aromatic compounds revealed that the *o*-, *m*- and *p*-xylene molecules are located in the channels in a pairwise fashion. The lattice constants of MIL-47 remained almost unchanged upon adsorption of *o*-, *m*- and *p*-xylene. Upon adsorption of EB, a severe change occurred in the lattice parameters of MIL-47. The ethyl groups prevented a similar planar alignment of two EB molecules in the channel.

Later, the same researchers thoroughly investigated the influence of the calcination parameters on the capacity and selectivity of MIL-47 for the *liquid-phase* adsorption of xylenes and other difunctionalized aromatics.[46] By varying the calcination time for the complete removal of the uncoordinated terephthalic acid from the pores and simultaneously avoiding oxidation to nonporous V_2O_5, pore volumes and uptake of xylenes were maximized. The presence of uncoordinated terephthalic acid

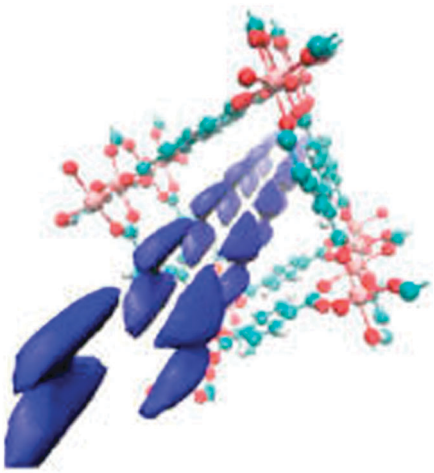

Fig. 11 Free energy isosurface at 5 kJ mol^{-1} showing low-energy regions for benzene in MIL-47 along a 2-fold screw axis. Reproduced with permission from ref. 42. Copyright 2012 American Chemical Society.

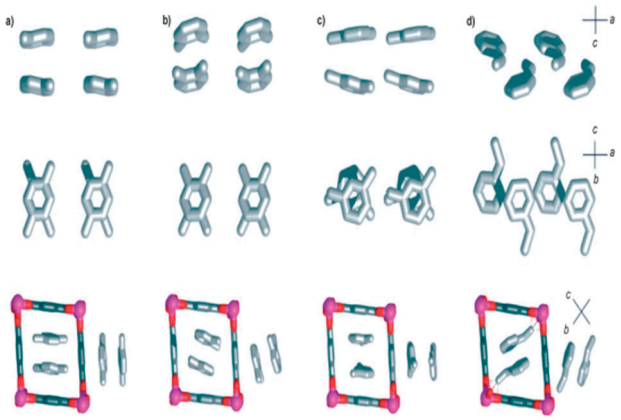

Fig. 12 Rietveldt refinements of MIL-47 crystals loaded with different C_8 alkylaromatic compounds: packing in the pores with (a) *p*-xylene, (b) *o*-xylene, (c) *m*-xylene and (d) ethylbenzene (color codes: gray, carbon; red, oxygen; pink, vanadium). All refinements were made in the space group *Pnma*. Reproduced with permission from ref. 44. Copyright 2007 Wiley-VCH Verlag GmbH & Co. KGaA.

in the channels increased the selectivity between *p*- and *m*-xylene. The *vapour-phase* adsorption and separation of xylenes and EB in MIL-47 was extensively investigated.[47] At very low partial pressure, the xylenes and EB showed comparable Henry adsorption constants and adsorption enthalpies. The relatively low value of the adsorption enthalpies on MIL-47 compared with those on zeolites indicated the easy regeneration of the former adsorbent at low energy cost. In spite of their comparable Henry adsorption constants and adsorption enthalpies, the individual C_8 alkylaromatics exhibited different adsorption capacities and isotherm shapes. The largest uptake value of 40 wt% (3.4 molecules per unit cell) at 70 °C was observed for *p*-xylene, which was in order followed by *o*-xylene, *m*-xylene and EB.

The *liquid-phase* adsorption and separation of styrene (ST) and EB in MIL-47 was compared with those of Al–MIL-53.[48] Competitive adsorption experiments revealed high selectivity of both materials for ST over EB. The styrene adsorption capacity of both materials reached ~20 wt%, which was similar to the value obtained in the single-component adsorption experiments under the same conditions. For MIL-47, the presence of EB in the mixture did not influence the adsorption of ST. The EB uptake in competitive experiments did not exceed 5 wt%, whereas up to 16 wt% of EB was adsorbed in the single component mode. For MIL-47, the separation factors were independent of temperature and the adsorption enthalpies of the two components (EB and ST) were similar. This indicated that the separation was governed by the entropic effect. Like xylenes, the Rietveldt refinement of the XRPD patterns of MIL-47 saturated with ST revealed that the molecules were packed in a pairwise manner in the channels. These findings have been confirmed recently by Ghysels *et al.* These authors have conducted an analysis of the xylene–MIL-47 framework and the xylene–xylene interactions using quantum chemical techniques.[49] They suggested that the separation properties should be mainly driven by entropy effects. Indeed, the mobility of the xylene isomers in both single and mixture components in such an MOF should be theoretically investigated by means of a molecular dynamics simulation to fully account for the dynamics of each single xylene isomer. In addition, to discriminate between the three xylene isomers, accurate host–guest interactions are needed to obtain a more pronounced discrimination between the self-diffusion coefficients. Guest–guest interactions are also important when considering the dynamics of mixed species in confinement. However, the selective adsorption of *para*-, *ortho*- and *meta* isomers of xylenes as observed experimentally has not yet been fully explained by theoretical calculations. Rives *et al.*[43] have shown the way to tackle this problem, and in particular the entropic effects, but a quest for more accurate force fields remains highly necessary in the near future, if we want to be able to reproduce theoretical selectivities as those observed for the xylene isomers in MIL-47.

Also, the liquid-phase adsorption and separation of *mono- and di-substituted alkylaromatics* in MIL-47 and Al–MIL-53 were investigated.[50] These uptakes corresponded to 0.08 and 0.49 molecules of cumene and *n*-propylbenzene, respectively. The separation factor between *n*-propylbenzene and cumene was 2.2 at room temperature.

The liquid-phase adsorption and separation of *naphthalene, alkylnaphthalenes and dichlorobenzenes* in MIL-47, Al–MIL-53 and $Cu_3(BTC)_2$ were also evaluated.[41] For naphthalene and alkylnaphthalenes, the competitive batch adsorption experiments in all the three MOFs displayed uptake values often higher than 20 wt%. The adsorption preferences were the same for all the three MOFs, with 1,4-dimethylnaphthalene preferred the least and 2-methylnaphthalene preferred the most. The fast elution of 1,4-dimethylnaphthalene compared to the other compounds indicated the size exclusion of this compound because of its largest kinetic diameter. For other compounds, the steric effects were not noticed, since naphthalene eluted much earlier than the monoalkylated naphthalenes. For dichlorobenzenes, the batch adsorption experiments exhibited total uptakes of 15 and 25 wt%, for MIL-47 and MIL-53, respectively. This difference was attributed to the polar nature of the Al–MIL-53 pores, in which the favourable interactions between the –OH groups in the pore walls and the polar adsorbates increased the uptake. In the pulse chromatographic experiments, $Cu_3(BTC)_2$ showed no separation of the dichlorobenzenes. Both MIL-47 and Al–MIL-53 showed the same elution order. The fast elution of *m*-dichlorobenzene was successively followed by the elution of *o*- and *p*-dichlorobenzenes. The breakthrough experiments involving *m*- and *p*-dicholorobenzene revealed that the separation factor was higher for Al–MIL-53 than for MIL-47.

The low-coverage adsorption properties of *aromatic and heterocyclic compounds* in MIL-47 were investigated by pulsed chromatographic experiments.[51] The 22 probe molecules included a set of benzene derivatives with alkyl, halogen and other functional groups and heterocyclic C_5–C_6 molecules. The effect of molecular functionality (mean polarizability, dipole moment, *etc.*) and size were found to correlate with the Henry adsorption constants and adsorption enthalpies of the probe molecules. A linear correlation (Fig. 13) between mean polarizability and adsorption enthalpy was obtained for most components. Both halogen and alkyl series followed the trend, indicating that the adsorption properties were the result of increased polarizability

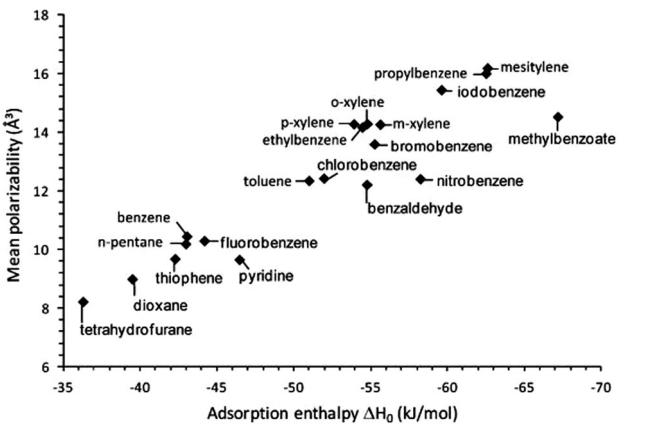

Fig. 13 Relationship between mean molecular polarizability and adsorption enthalpy for aromatic and heterocyclic compounds in MIL-47 at zero coverage. Reproduced with permission from ref. 51. Copyright 2012 American Chemical Society.

and not due to the higher electronegativity of the halogen atoms. The compounds with oxygen-containing functional groups (benzaldehyde, nitrobenzene and methylbenzoate) deviated from the trend.

Besides vanadium-MOFs with (V═O–V═O) chains that contain no saturated metal sites, vanadium-MOFs constructed with inorganic V_3O trimers contain unsaturated V-sites that are ideal for the selective adsorption of specific compounds. Recently, Van de Voorde *et al.* demonstrated that V–MIL-100 is very selective for the removal of nitrogen containing contaminants from fuels compared to other MIL-100 variants.[52] It outperforms the previously suggested MIL-100(Fe), but also the Al and Cr variants. When properly pretreated, MIL-100(V) has a similar capacity as the other variants, but a higher selectivity and affinity for the N-containing contaminants. The driving force is analysed as enthalpic, through coordination of the adsorbates with the unsaturated V-centers. Furthermore, MIL-100(V) was also compared with MIL-100(Fe) and MIL-100(Cr) in a screening study for high pressure gas sorption.[53] The authors noticed however large differences between several MIL-100(V) batches, indicating a large dependence of the material characteristics on small deviations in synthesis procedure. This was also noticed for other metal-nodes.

Concluding remarks and perspectives

This paper gives a state of the art overview of the different types of V-MOFs and their applications in adsorption, separation and catalysis. In spite of the fact that vanadium is able to form several stable clusters, only a few MOFs have been reported in which the V is actually present as an oxide cluster. Out of the dozen V-MOFs listed in Table 1, almost all the studies are devoted to MIL-47. Most of the other reported V-MOFs lack either the open porosity or the structural and chemical stability to withstand the experimental conditions of catalysis and sorption. Very recently, MIL-100(V), which is significantly more stable than the MIL-101(V), is gaining interest as a selective adsorbent. It outperforms the other variants (Cr, Fe, Al) in base sorption, as the V(III) site is believed to have a higher Lewis acidity and a higher affinity for N/S heterocyclic molecules. The COMOC-2 shows interesting breathing properties, and might open interesting perspectives towards new applications as they behave as the isoreticular flexible variants of the MIL-53. Still, we expect that new structures will be proposed, or at least the V-variant of other topologies. Stability is of course always a conditional property: the materials should be stable in the conditions they are used and not necessarily in air, although complications in storage and handling are not beneficial.

MIL-47 has been extensively studied in epoxidation catalysis, both experimentally and theoretically. Although the parent material has completely saturated sites, the catalyst is remarkably active after an initial selective breaking of some of the V–O bonds. Conditions can be found, mostly waterfree, in which the catalyst is structurally stable and does not leach. This opens perspectives towards the development of even more active and selective catalysts, by controlling the coordination of the V-sites. This has already been done for other MOF-systems, for instance the Zr-containing UiO-66, using so-called modulators.[54] These modulators are not bifunctional, such as terephthalic acid, but mono-acids, such as acetic acid. This way, the number of defect sites can be controlled. The open tunnel-like pores of the MIL-47 structure allow very fast transport of reagents or products and can be tuned in size. Our current studies in catalysis on MIL-47 have shown that a significant fraction of V–O bonds can be broken without a dramatic loss in stability.

Another interesting route of synthesizing more active and stable V-catalysts based on MOFs is to dope a more stable and/or inert structure (*e.g.* MIL-53) selectively with V-sites. This way, one could imagine that "distant" catalytic sites are created. Focusing on the adsorption behavior, a first publication on a mixed (V,Fe)–MIL-53 structure has been reported by the Walton group.[55] They could show a true "atomic" mixing of the Fe(III)/V(III) sites. We expect that more work in this direction will be reported in the near future, as it is an elegant way to tune the catalytic properties, as well as sorption behavior.

Adsorption and separation are sometimes believed to be the main areas of application of MOFs. The V-MOFs form no exception. Many experimental and theoretical studies are devoted to the interactions of all kinds of hydrocarbons, but also CO_2, N_2, nitrogen and sulphur containing molecules with the MOF matrix. In most cases, the MIL-47 is tested as the adsorbent and in most studies, the saturated V-sites form no real contribution to the selectivity or the affinity of the adsorbent. The most important contribution of the V^{IV}-node is to keep the structure rigid in typical sorption conditions, contrary to the M^{III}–MIL-53(Al, Cr, Fe) isotopical variants. MIL-47 has a very high CO_2 uptake capacity, compared to the MIL-53 variants. For aromatics, the important governing factors are confinement effects and pi–pi and stacking interactions with the aromatic system in the terephthalic linkers. Functionalization of the linkers can improve the selectivity of the material in gas separation. The uncoordinated metal-sites are important in the MIL-100(V), as it has been shown that this structure outperforms the other metal variants (Fe, Cr) in the selective adsorption of N or S containing hydrocyclic fuel contaminants. Only a few reports have appeared on MIL-100(V), we might see more adsorption studies in the future on this promising material.

MIL-47(V) differs strongly from the isotopical MIL-53(Al, Cr) in structural flexibility. Whereas MIL-47 under mild working conditions is "rigid", the MIL-53 variant "breathes". It is a very complex interplay of different factors: the structural flexibility completely reverses when enlarging the linker, as in naphthalene or diphenyl linkers. These Al(III)-MOFs, denoted as DUT-4 and DUT-5 are rigid, whereas the V(IV) variant, denotes as COMOC-2 is flexible. The reasons are not yet fully understood. A combined experimental and theoretical effort is needed to "predict" and rationalize the breathing behavior of MOFs. Huge progress is currently being made in the development of theoretical models and force fields to model the interaction of the MOF frameworks with guest molecules. Operando spectroscopy might prove to be invaluable in the further development

of this knowledge. A full understanding of structural flexibility is one of the main challenges to be addressed in the near future by the MOF society.

List of acronyms and abbreviations

AC	Active complex
2D	Two-dimensional
3D	Three-dimensional
AS	As-synthesized
BDC	1,4-Benzenedicarboxylic acid
BDC-NH_2	2-Aminoterephthalate
BET	Brunauer–Emmett–Teller
BPDC	Biphenyl-4,4′-dicarboxylate
BT	Benzothiophene
BTC	1,3,5-Benzenetricarboxylate
BTEC	1,2,4,5-Benzenetetracarboxylate
COMOC	Center for Ordered Materials, Organometallics and Catalysis
DMF	*N*,*N*′-Dimethylformamide
DUT	Dresden University of Technology
EB	Ethylbenzene
EPR	Electron paramagnetic resonance
GCMC	Grand-canonical Monte Carlo
IAST	Ideal adsorbed solution theory
IC	Inactive complex
IGCC	Integrated gasification combined cycle
LP	Large pore
MD	Molecular dynamics
MIL	Material of Institute Lavoisier
MOF	Metal–organic framework
NDC	2,6-Naphthalenedicarboxylate
NP	Narrow pore
PSA	Pressure swing adsorption
QENS	Quasi-elastic neutron scattering
ST	Styrene
VST	Vacancy solution theory
XRPD	X-ray powder diffraction

Acknowledgements

The authors acknowledge the financial support from the Ghent University BOF postdoctoral grants 01P02911T (YYL) and 01P068135 (K.L), and BOF PhD grant 01D31608 (MVD) and UGent GOA Grant 01G00710. We acknowledge the Long Term Structural Methusalem Grant 01M00409. The authors are grateful to the Research Foundation Flanders (FWO), the Research Board of Ghent University, and BELSPO in the frame of IAP P7/05. Funding was also received from the European Research Council under the European Community's Seventh Framework Program [FP7(2007–2013) ERC grant agreement number 240483]. We thank Dr Matthias Ide for his help with the graphics. Computational resources and services used in this work were provided by the Stevin Supercomputer Infrastructure of Ghent University.

References

1 K. Barthelet, J. Marrot, D. Riou and G. Ferey, *Angew. Chem., Int. Ed.*, 2002, **41**, 281.
2 I. J. Kang, N. A. Khan, E. Haque and S. H. Jhung, *Chem.–Eur. J.*, 2011, **17**, 6437.
3 X. Wang, L. Liu and A. J. Jacobson, *Angew. Chem., Int. Ed.*, 2006, **45**, 6499.
4 A. Phan, A. U. Czaja, F. Gandara, C. B. Knobler and O. M. Yaghi, *Inorg. Chem.*, 2011, **50**, 7388.
5 K. Barthelet, D. Riou and G. Ferey, *Chem. Commun.*, 2002, 1492.
6 K. Barthelet, J. Marrot, G. Ferey and D. Riou, *Chem. Commun.*, 2004, 520.
7 K. Barthelet, D. Riou, M. Nogues and G. Ferey, *Inorg. Chem.*, 2003, **42**, 1739.
8 K. Barthelet, K. Adil, F. Millange, C. Serre, D. Riou and G. Ferey, *J. Mater. Chem.*, 2003, **13**, 2208.
9 Y.-Y. Liu, S. Couck, M. Vandichel, M. Grzywa, K. Leus, S. Biswas, D. Vollmer, J. Gascon, F. Kapteijn, J. F. M. Denayer, M. Waroquier, V. Van Speybroeck and P. Van der Voort, *Inorg. Chem.*, 2013, **52**, 113.
10 Y. Y. Liu, K. Leus, M. Grzywa, D. Weinberger, K. Strubbe, H. Vrielinck, R. Van Deun, D. Volkmer, V. Van Speybroeck and P. Van der Voort, *Eur. J. Inorg. Chem.*, 2012, 2819.
11 A. Lieb, H. Leclerc, T. Devic, C. Serre, I. Margiolaki, F. Mahjoubi, J. S. Lee, A. Vimont, M. Daturi and J.-S. Chang, *Microporous Mesoporous Mater.*, 2012, **157**, 18.
12 S. Biswas, S. Couck, M. Grzywa, J. F. M. Denayer, D. Volkmer and P. Van der Voort, *Eur. J. Inorg. Chem.*, 2012, 2481.
13 T. Loiseau, C. Mellot-Draznieks, H. Muguerra, G. Ferey, M. Haouas and F. Taulelle, *C. R. Chim.*, 2005, **8**, 765.
14 G. Férey and C. Serre, *Chem. Soc. Rev.*, 2009, **38**, 1380.
15 H. Leclerc, T. Devic, S. Devautour-Vinot, P. Bazin, N. Audebrand, G. Ferey, M. Daturi, A. Vimont and G. Clet, *J. Phys. Chem. C*, 2011, **115**, 19828.
16 P. G. Yot, Q. Ma, J. Haines, Q. Yang, A. Ghoufi, T. Devic, C. Serre, V. Dmitriev, G. Ferey, C. Zhong and G. Maurin, *Chem. Sci.*, 2012, **3**, 1100.
17 I. Senkovska, F. Hoffmann, M. Fröba, J. Getzschmann, W. Böhlmann and S. Kaskel, *Microporous Mesoporous Mater.*, 2009, **122**, 93.
18 A. Ghysels, L. Vanduyfhuys, M. Vandichel, M. Waroquier, V. Van Speybroeck and B. Smit, *J. Phys. Chem. C*, 2013, **117**, 11540.
19 A. U. Ortiz, A. Boutin, A. H. Fuchs and F. X. Coudert, *Phys. Rev. Lett.*, 2012, **109**, 195502.
20 (*a*) K. Leus, I. Muylaert, M. Vandichel, G. B. Marin, M. Waroquier, V. Van Speybroeck and P. Van der Voort, *Chem. Commun.*, 2010, **46**, 5085; (*b*) K. Leus, I. Muylaert, V. Van Speybroeck, G. B. Marin and P. Van der Voort, in Scientific Bases for the Preparation of Heterogeneous Catalysts: Proceedings of the 10th International Symposium ed. E. M. Gaigneaux, M. Devillers, S. Hermans, P. A. Jacobs, J. A. Martens and P. Ruiz, 2010, vol. 175.
21 K. Leus, M. Vandichel, Y.-Y. Liu, I. Muylaert, J. Musschoot, S. Pyl, H. Vrielinck, F. Callens, G. B. Marin, C. Detavernier,

P. V. Wiper, Y. Z. Khimyak, M. Waroquier, V. Van Speybroeck and P. Van der Voort, *J. Catal.*, 2012, **285**, 196.
22 M. Vandichel, K. Leus, P. Van der Voort, M. Waroquier and V. Van Speybroeck, *J. Catal.*, 2012, **294**, 1.
23 K. Leus, G. Vanhaelewyn, T. Bogaerts, Y. Y. Liu, D. Esquivel, F. Callens, G. B. Marin, V. Van Speybroeck, H. Vrielinck and P. Van Der Voort, *Catal. Today*, 2013, **208**, 97.
24 S. Bourrelly, P. L. Llewellyn, C. Serre, F. Millange, T. Loiseau and G. Ferey, *J. Am. Chem. Soc.*, 2005, **127**, 13519.
25 (*a*) N. A. Ramsahye, G. Maurin, S. Bourrelly, P. L. Llewellyn, T. Devic, C. Serre, T. Loiseau and G. Ferey, *Adsorption*, 2007, **13**, 461; (*b*) N. A. Ramsahye, G. Maurin, S. Bourrelly, P. L. Llewellyn, C. Serre, T. Loiseau, T. Devic and G. Ferey, *J. Phys. Chem. C*, 2008, **112**, 514.
26 P. L. Llewellyn, S. Bourrelly, C. Vagner, N. Heymans, H. Leclerc, A. Ghoufi, P. Bazin, A. Vimont, M. Daturi, T. Devic, C. Serre, G. De Weireld and G. Maurin, *J. Phys. Chem. C*, 2013, **117**, 962.
27 K. Leus, S. Couck, M. Vandichel, G. Vanhaelewyn, Y.-Y. Liu, G. B. Marin, I. Van Driessche, D. Depla, M. Waroquier, V. Van Speybroeck, J. F. M. Denayer and P. Van Der Voort, *Phys. Chem. Chem. Phys.*, 2012, **14**, 15562.
28 S. Biswas, T. Remy, S. Couck, D. Denysenko, G. Rampelberg, J. F. M. Denayer, D. Volkmer, C. Detavernier and P. Van Der Voort, *Phys. Chem. Chem. Phys.*, 2013, **15**, 3552.
29 S. Biswas, D. E. P. Vanpoucke, T. Verstraelen, M. Vandichel, S. Couck, K. Leus, Y.-Y. Liu, M. Waroquier, V. Van Speybroeck, J. F. M. Denayer and P. Van Der Voort, *J. Phys. Chem. C*, 2013, **117**, 22784.
30 N. Rosenbach Jr., A. Ghoufi, I. Deroche, P. L. Llewellyn, T. Devic, S. Bourrelly, C. Serre, G. Ferey and G. Maurin, *Phys. Chem. Chem. Phys.*, 2010, **12**, 6428.
31 P. Serra-Crespo, E. V. Ramos-Fernandez, J. Gascon and F. Kapteijn, *Chem. Mater.*, 2011, **23**, 2565.
32 S. Couck, J. F. M. Denayer, G. V. Baron, T. Remy, J. Gascon and F. Kapteijn, *J. Am. Chem. Soc.*, 2009, **131**, 6326.
33 L. Hamon, N. Heymans, P. L. Llewellyn, V. Guillerm, A. Ghoufi, S. Vaesen, G. Maurin, C. Serre, G. De Weireld and G. D. Pirngruber, *Dalton Trans.*, 2012, **41**, 4052.
34 G. D. Pirngruber, L. Hamon, S. Bourrelly, P. L. Llewellyn, E. Lenoir, V. Guillerm, C. Serre and T. Devic, *ChemSusChem*, 2012, **5**, 762.
35 N. Rosenbach, H. Jobic, A. Ghoufi, F. Salles, G. Maurin, S. Bourrelly, P. L. Llewellyn, T. Devic, C. Serre and G. Ferey, *Angew. Chem., Int. Ed.*, 2008, **47**, 6611.
36 T. K. Trung, I. Deroche, A. Rivera, Q. Yang, P. Yot, N. Ramsahye, S. D. Vinot, T. Devic, P. Horcajada, C. Serre, G. Maurin and P. Trens, *Microporous Mesoporous Mater.*, 2011, **140**, 114.
37 I. Deroche, S. Rives, T. Trung, Q. Yang, A. Ghoufi, N. A. Ramsahye, P. Trens, F. Fajula, T. Devic, C. Serre, G. Ferey, H. Jobic and G. Maurin, *J. Phys. Chem. C*, 2011, **115**, 13868.
38 T. K. Trung, P. Trens, N. Tanchoux, S. Bourrelly, P. L. Llewellyn, S. Loera-Serna, C. Serre, T. Loiseau, F. Fajula and G. Férey, *J. Am. Chem. Soc.*, 2008, **130**, 16926.
39 S. Biswas, S. Couck, D. Denysenko, A. Bhunia, M. Grzywa, J. F. M. Denayer, D. Volkmer, C. Janiak and P. Van Der Voort, *Microporous Mesoporous Mater.*, 2013, **181**, 175.
40 V. Finsy, S. Calero, E. Garcia-Perez, P. J. Merkling, G. Vedts, D. E. De Vos, G. V. Baron and J. F. M. Denayer, *Phys. Chem. Chem. Phys.*, 2009, **11**, 3515.
41 L. Alaerts, M. Maes, M. A. van der Veen, P. A. Jacobs and D. E. De Vos, *Phys. Chem. Chem. Phys.*, 2009, **11**, 2903.
42 D. I. Kolokolov, H. Jobic, A. G. Stepanov, J. Ollivier, S. Rives, G. Maurin, T. Devic, C. Serre and G. Ferey, *J. Phys. Chem. C*, 2012, **116**, 15093.
43 S. Rives, H. Jobic, D. I. Kolokolov, A. A. Gabrienko, A. G. Stepanov, Y. Ke, B. Frick, T. Devic, G. Ferey and G. Maurin, *J. Phys. Chem. C*, 2013, **117**, 6293.
44 L. Alaerts, C. E. A. Kirschhock, M. Maes, M. A. van der Veen, V. Finsy, A. Depla, J. A. Martens, G. V. Baron, P. A. Jacobs, J. E. M. Denayer and D. E. De Vos, *Angew. Chem., Int. Ed.*, 2007, **46**, 4293.
45 J. M. Castillo, T. J. H. Vlugt and S. Calero, *J. Phys. Chem. C*, 2009, **113**, 20869.
46 L. Alaerts, M. Maes, P. A. Jacobs, J. F. M. Denayer and D. E. De Vos, *Phys. Chem. Chem. Phys.*, 2008, **10**, 2979.
47 V. Finsy, H. Verelst, L. Alaerts, D. De Vos, P. A. Jacobs, G. V. Baron and J. F. M. Denayer, *J. Am. Chem. Soc.*, 2008, **130**, 7110.
48 M. Maes, F. Vermoortele, L. Alaerts, S. Couck, C. E. A. Kirschhock, J. F. M. Denayer and D. E. De Vos, *J. Am. Chem. Soc.*, 2010, **132**, 15277.
49 A. Ghysels, M. Vandichel, T. Verstraelen, M. A. van der Veen, D. E. De Vos, M. Waroquier and V. Van Speybroeck, *Theor. Chem. Acc.*, 2012, **131**, 1234.
50 M. Maes, F. Vermoortele, M. Boulhout, T. Boudewijns, C. Kirschhock, R. Ameloot, I. Beurroies, R. Denoyel and D. E. De Vos, *Microporous Mesoporous Mater.*, 2012, **157**, 82.
51 T. Duerinck, S. Couck, F. Vermoortele, D. E. De Vos, G. V. Baron and J. F. M. Denayer, *Langmuir*, 2012, **28**, 13883.
52 B. Van de Voorde, M. Boulhout, F. Vermoortele, P. Horcajada, D. Cunha, J. S. Lee, J. S. Chang, E. Gibson, M. Daturi, J. C. Lavalley, A. Vimont, I. Beurroies and D. E. De Vos, *J. Am. Chem. Soc.*, 2013, **135**, 9849.
53 A. D. Wiersum, C. Gioyannangeli, D. Vincent, E. Bloch, H. Reinsch, N. Stock, J. S. Lee, J. S. Chang and P. L. Llewellyn, *ACS Comb. Sci.*, 2013, **15**, 111.
54 (*a*) F. Vermoortele, M. Vandichel, B. Van de Voorde, R. Ameloot, M. Waroquier, V. Van Speybroeck and D. E. De Vos, *Angew. Chem., Int. Ed.*, 2012, **51**, 4887; (*b*) F. Vermoortele, B. Bueken, G. Le Bars, B. Van de Voorde, M. Vandichel, K. Houthoofd, A. Vimont, M. Daturi, M. Waroquier, V. Van Speybroeck, C. Kirschhock and D. E. De Vos, *J. Am. Chem. Soc.*, 2013, **135**, 11465.
55 M. I. Breeze, G. Clet, B. C. Campo, A. Vimont, M. Daturi, J.-M. Grenèche, A. J. Dent, F. Millange and R. I. Walton, *Inorg. Chem.*, 2013, **52**, 8171.